Journal of Applied Polymer Science

Long-Range-Ordered, Hexagonally Packed Nanoporous Membranes from Degradable-Block-Containing Diblock Copolymer Film Templates

Lei Lei, Yuzheng Xia, Xiaonong Chen, Shuxian Shi

Key Laboratory of Carbon Fiber and Functional Polymers (Ministry of Education), Beijing University of Chemical Technology, Beijing 100029, China

Correspondence to: S. Shi (E-mail: shisx@mail.buct.edu.cn)

ABSTRACT: Polystyrene (PS)-*b*-polylactide (PLA) diblock copolymers with different molecular weights and fractions were synthesized through a combination of living anionic polymerization and controlled ring-opening polymerization. Then, the PS–PLA films were guided to phase-separate by self-assembly into different morphologies through casting solvent selection, solvent evaporation, and thermal and solvent-field regulation. Finally, perpendicularly oriented PS–PLA films were used as precursors for PS membranes with an ordered periodic nanoporous structure; this was achieved by the selective etching of the segregated PLA domains dispersed in a continuous matrix of PS. Testing techniques, including IR, ^{1}H-NMR, gel permeation chromatography, scanning electron microscopy (SEM), and atomic force microscopy (AFM), were used to determine the chemical structure of the PS–PLA copolymer and its film morphology. AFM images of the self-assembled PS-PLA films indicate that vertical tapers of the PLA domains were generated among PS continuum when either toluene or tetrahydrofuran was used as the annealing solvent. The SEM images certified that the chemical etching of the PLA component from the self-assembled PS–PLA films led to a long-range-ordered array of hexagonally packed nanoporous membranes with a diameter about 500 nm and a center-to-center distance of 1700 nm. © 2013 Wiley Periodicals, Inc. J. Appl. Polym. Sci. **2014**, *131*, 39638.

KEYWORDS: biodegradable; copolymers; membranes; polystyrene; self-assembly

Received 1 February 2013; accepted 3 June 2013

DOI: 10.1002/app.39638

INTRODUCTION

Block copolymers (BCPs) formed by covalently linked segments spontaneously self-assemble into microphase-separation structures because of the distinct chemical properties between the constituent blocks; this leads to different phase-separation morphologies.[1] The classic phase-separation structures formed by BCPs are body-centered cubic spheres, hexagonally packed cylinders, gyroids, and lamellae,[2] which often display a regular periodic order with a repeat distance of about 10–100 nm.[3] Typically, some of these nanostructures have proven particularly advantageous for ideal templates where large-area patterns of nanoscale features are desired.[4–6] Specifically, a vertical-column morphology ($C_\perp$) in a nanoporous membrane derived from BCPs makes an attractive candidate for liquid separation[7,8] and drug delivery[9,10] because of its tunable pore size and long-range-ordered distribution.

The precursors of nanoporous membranes are always prepared by spin-coating technology, in which the film thickness can be regulated by alteration of the concentration of casting solution or rotation speed.[11] The final morphology of self-assembling BCPs depends on the competitive balance between the interphase forces and the stretching interactions among contiguous blocks, whereas the size and periodicity of the phase-separation microdomains are mainly affected by molecular parameters, such as the interaction parameter (χ), the degree of polymerization, and the block volume fraction.[12,13] For BCP films, extra factors, such as film thickness and polymer/substrate (or free surface) interactions, will be involved; these make the self-assembling system more complicated.[14]

Although an ordered phase-separation morphology can be obtained with mere reliance on the self-assembly features of the block polymer, multiple inducement techniques, such as electric fields,[15] mechanical strain,[16] solvent annealing,[17] and thermal annealing,[18] have always been applied to better meet the demands of large-scale, high-strength, orientation and defect-free requirements for nanolithographic applications. Among these multifarious inducements, thermal annealing is thought to be the most direct way to regulate the assembly of BCPs; one usually conducts it by heating the BCPs above the highest glass-transition temperature (T_g) of the components and thus providing the polymer chains with enough energy to regulate their

conformation and orientation.[19,20] However, thermal annealing is always prohibited by the prodigious viscosity between the polymer chains or the relatively narrow temperature window between the highest T_g and the lowest thermal degradation temperature of the BCPs, especially for PLA-containing polymers.[3,21] Therefore, solvent annealing in selective or neutral solvents has become a prominent route for the regulation of the self-assembling process of BCPs where thermal treatment acts are infeasible for achieving thermal equilibrium.[22,23] Solvent-annealing theories based on well-established polymer physicochemical properties[6,24] indicate that the polymer–solvent interaction parameters (χ_{P-S}'s), polymer composition, and solvent extraction mechanics are effective factors for manipulating the morphology and orientation of self-assembling BCP films.[25–27] For instance, perpendicularly oriented cylinder phase-separation structures have been achieved in BCP films through the adjustment of the solvent-evaporation rates or by solvent-annealing approaches.[7,10,28,29] These studies have shown that the evaporation of the solvent from BCP films kinetically traps the cylinder phase-separation structures to orient perpendicularly, and blocks with a lower surface energy tend to accumulate parallel to the free surface.

Transformation reactions in polymerization, which were proposed by Richards et al.[30] in 1976, can effectively handle monomers with different mechanisms, especially copolymers with distinct block structures. They make up for the disadvantages of monotonous product properties in ordinary polymerization and generate functional polymers with a variety of structures and properties. For instance, PLA containing BCPs, which combine biodegradable and self-assembling properties, have been investigated extensively for biomedical[31] and engineering materials.[32–34]

In this study, asymmetric polystyrene (PS)-polylactide (PLA) diblock copolymers with different PLA fractions (f_{PLA}'s) were prepared through a transformation from living anionic polymerization to controlled ring-opening polymerization. Subsequently, external inducements, such as thermal and solvent fields, were progressively introduced to regulate the self-assembling process of the PS–PLA films and to pursue a vertical-column phase-separation morphology. A micelle-fusion model was used to predict the self-assembling behavior of PS–PLA in selective solvents along with solvent evaporation. Both toluene (the selective solvent for validation) and chloroform (which was neutral for comparison) were chosen as the casting solvents to regulate the self-assembling behavior of PS–PLA through solvent evaporation. Moreover, the solvent-annealing method was applied to the PS–PLA films in a saturated toluene- or tetrahydrofuran (THF)-vapor atmosphere to precisely regulate its final surface morphologies. The chemical etching of the PLA segment from self-assembled PS–PLA films was applied, and long-range-ordered nanoporous membranes were achieved in this way. The effects of f_{PLA} on the morphologies of the PS–PLA films and the pore size of the PLA etched membranes were investigated.

EXPERIMENTAL

Materials

All of the styrene (≧98.0%, Fuchen Chemical Reagent Co., Ltd.) was purified by stirring overnight with calcium hydride (CaH_2, Sinopharm Chemical Reagent Co., Ltd.) followed by vacuum distillation at about 30°C; then it was stored under nitrogen, and a little piece of sodium was used to remove the trace water. Ethylene oxide (EO; ≧99.5%, Sinopharm Chemical Reagent Co., Ltd.) was refined by stirring overnight with CaH_2 and distilled at 16°C, and then it was sealed by cryopreservation. *n*-Butyllithium (*n*-BuLi; TCI Shanghai Co., Ltd.) was dissolved in cyclohexane with a concentration of 1.6*M* and triethylaluminum ($AlEt_3$; Sun Chemical Technology Co., Ltd.) in toluene with a concentration of 2.0*M;* both of these were used as received and were stored in a nitrogen atmosphere at about 7°C. The purification of cyclohexane and toluene (≧99.5%, Beijing Chemical Reagent Co., Ltd.) were carried out by stirring overnight with CaH_2 and distillation. They were dried further with a little piece of sodium immersed during storage. D,L-Lactide (≧99.5%, Jinan Daigang Biomaterial Co., Ltd.) was purified by recrystallization from acetic ether three times and dried *in vacuo* at room temperature. Then it was sealed under a nitrogen atmosphere and conserved in a desiccator.

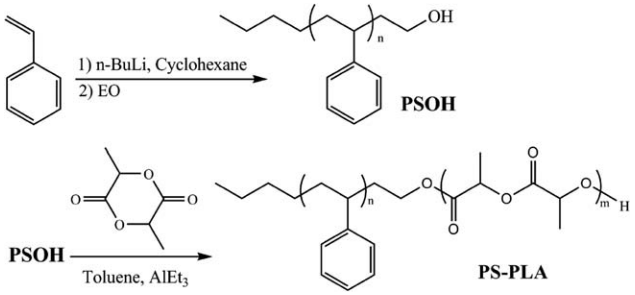

Figure 1. Synthetic route of the PS–PLA diblock copolymer.

Synthesis of PS–PLA

In this study, all of the PS–PLA samples were prepared through a combination of living anionic polymerization and controlled ring-opening polymerization (Figure 1). First, *n*-BuLi was applied as the initiator, and EO was applied as the block-ending agent to obtain hydroxyl-terminated polystyrene (PSOH). Then, equimolar amounts of $AlEt_3$ and PSOH were used to generate an aluminum alkoxide macroinitiator to initiate D,L-lactide for the preparation of PS–PLA. A representative experimental operation is described as follows.

An example for the synthesis of $PS_{40900}OH$ is described here. The polymerization was performed in a 250-mL flask accessorized with a reagent inlet connected to a rubber catheter, which was clamped on the other end. All of the reagents were introduced by a gastight syringe under nitrogen protection. Before the injection of cyclohexane, the degassed flask was flame-dried and degased with nitrogen to ensure that the system was anhydrous and oxygen-free. An appropriate amount of *n*-BuLi was used to deplete the impurity of cyclohexane (130 mL), and the system gradually turned from colorless to pale yellow. A calculated amount of *n*-BuLi (0.35 mL, 5.48×10^{-4} mol) was injected to the system, which became red-orange after styrene (23.56 g, 2.27×10^{-1} mol) was added at a steady rate; then the solution was stirred at 50°C for 5 h. The mixture was cooled to room temperature before the addition of EO (1.25 mL, 2.47 ×

10^{-2} mol), after which the mixture became colorless. Specifically, the syringe was cooled in liquid nitrogen; otherwise, EO would have soon evaporated. The reaction system was stirred at room temperature for another 12 h, and the reaction was terminated by the injection of 5 mL of ethanol. The product was precipitated in ethanol and dried *in vacuo* at 40°C for 24 h. Finally, a white powder PSOH with a yield of 24.44 g (98.07%) was obtained. The molecular weight of the PSOH was 43.7 kg/mol, as determined by end-group analysis from ^{1}H-NMR spectra; this was almost identical to the 40.9 kg/mol determined by gel permeation chromatography (GPC), and both were close to the targeted number-average molecular weight (M_n) of 43 kg/mol. The GPC results gave a M_w/M_n value of 1.37.

For the synthesis of PS_{40900}–PLA_{4600}, all of the experimental apparatus were preserved from the PSOH preparation unless cyclohexane was replaced by toluene as the solvent. Specifically, PSOH ($M_n = 40.9$ kg/mol, 5.00 g, 1.22×10^{-4} mol) and degassed toluene (40 mL) were added to a 250-mL flame-dried and oxygen-free flask. Then, $AlEt_3$ (0.061 mL, 1.22×10^{-4} mol) was injected into the system and stirred at room temperature for 12 h to form the aluminum alkoxide macroinitiator. Then, D,L-lactide (1.0 g, 6.94×10^{-3} mol) was dissolved in hot toluene under nitrogen protection and injected into the reaction system as quickly as possible in case D,L-lactide crystallized from toluene at a relatively low temperature. The flask was stirred at 80°C for 24 h, after which 5 mL of ethanol was injected to terminate the reaction system. The product was precipitated in excess ethanol and dried *in vacuo* at 40°C for 24 h. The block polymer was characterized by GPC analysis (45.5 kg/mol, $M_w/M_n = 1.29$) and ^{1}H-NMR spectra ($M_n = 47.3$ kg/mol, $f_{PLA} = 10.11\%$).

Preparation of the PS–PLA Film Samples

A series of asymmetric PS–PLA samples (PS_{3900}–PLA_{3800}, PS_{20000}–PLA_{10000}, PS_{40900}–PLA_{4600}, PS_{14300}–PLA_{6000}, and PS_{14300}–PLA_{3700}) were used as raw materials for the PS–PLA films. All of the PS–PLA film samples were prepared by spin-coating. The PS–PLA/solvent solution, with a concentration of 0.1 g/mL, was spin-coated onto silicon wafers (5×5 mm^2) at 400 rpm for 9 s first and at 2000 rpm for 40 s later. The qualified PS–PLA films displayed a flat surface without any corrugated profile which would generate rainbowlike optical interference under sunshine. Before spin-coating, the wafers were pretreated in a 70:30 v/v solution of 98% H_2SO_4 and 30% H_2O_2 at 80°C for 45 min to generate an SiO_x layer on the silicon surface. Then, the wafers were cleaned with sonication in deionized water and acetone, respectively, for 10 min and dried thoroughly.

Self-Assembly of the PS–PLA Films

The self-assembling phase-separation structure of the PS–PLA films were regulated by thermal and solvent fields, respectively. The surface morphology of the self-assembled PS–PLA films was characterized by atomic force microscopy (AFM) and scanning electron microscopy (SEM).

Thermal-Field Regulation System. A thermal field was applied to regulate the self-assembling structure of the asymmetric PS–PLA films. The resulting surface morphology of the self-assembled PS–PLA films was reflected by SEM images of the PLA-etched PS–PLA film samples. The PS–PLA films were prepared by spin-coating, during which the PS–PLA/chloroform solution (0.1 g/mL) was spin-coated onto silicon wafers and then desiccated *in vacuo* at 25°C for 24 h.

Ovens maintaining constant temperatures (110, 125, or 140°C) were used for thermal annealing. The PS–PLA films were implanted and thermally annealed at different temperatures for 4 and 9 h, respectively. The self-assembled PS–PLA films were immersed in a 0.5*M* alkaline solution (methanol/water = 2:3 v/v) at 60°C for 7 days to hydrolyze the PLA component. The PS–PLA films peeled from the substrate were washed with water and methanol, respectively, and dried *in vacuo* for SEM characterization.

Solvent-Field Regulation System. The solvent-field regulation of the self-assembling PS–PLA films was mainly focused on the selection of the casting solvent and solvent annealing. Both neutral and selective solvents were used to cast the PS–PLA films according to their χ_{P-S}'s. Solvent steam was used to fumigate the PS–PLA films, and this is known as the *solvent-annealing process*.

The effect of solvent selection on the self-assembling PS–PLA films was investigated by the spin-coating of PS–PLA with different coating solvents (toluene and chloroform) and the evaporation of the residual solvent at 25°C in open air. Solvent annealing was performed by exposure of the PS–PLA films to different solvent-vapor atmospheres (toluene, acetone, and THF) at 40°C for different periods (5, 7, 12, and 24 h). Closed beakers (50 mL) reserved with 15 mL of different solvents were thermostated at 40°C to create stable solvent-evaporation circumstances. Both solvent-evaporation- and solvent-annealing-treated PS–PLA films were immersed in liquid nitrogen to stabilize the self-assembled structures. The surface morphologies of the PS–PLA films were detected by AFM.

Etching of PLA from the Self-Assembled PS–PLA Films

We conducted the degradation of PLA by soaking the self-assembled PS–PLA films in a 0.5*M* alkaline solution, which was prepared by the dissolution of 2.0 g of sodium hydroxide in a 2:3 v/v solution of methanol and water. The etching process was performed at 40°C and lasted for 15 days. After etching, the PS–PLA film peeled from the substrate was fished out and rinsed with deionized water and methanol, respectively, and then, the PS–PLA films were dried *in vacuo* for SEM characterization.

Characterization

All of the ^{1}H-NMR spectra were recorded on an AV600 NMR spectrometer (Bruker Optics). The PSOH and PS–PLA samples were dissolved in deuterated chloroform with a concentration of 1 wt % for NMR analysis. The IR spectral analysis of the polymer powder was performed directly on a Thermo Nicolet 6700 IR spectrometer. The molecular weights were characterized by a Waters 150C gel permeation chromatograph, during which the PSOH and PS–PLA samples were dissolved in THF with a concentration of roughly 2–4 mg/mL and characterized at 30°C. The thermodynamic properties of PS–PLA were scanned by

Table I. Characterization of the PSOH and PS–PLA Samples

PSOH				PS–PLA				
Macroinitiator	M_n (kg/mol)[a]	M_w/M_n[b]	M_n (kg/mol)[c]	BCP	M_n (kg/mol)[a]	M_w/M_n[b]	M_n(PLA) (kg/mol)[d]	f_{PLA} (%)[e]
$PS_{3900}OH$	3.9	1.13	4.6	PS_{3900}-PLA_{3800}	7.7	1.34	3.8	49.35
$PS_{14300}OH$	14.3	1.31	16.1	PS_{14300}-PLA_{6000}	20.3	1.15	6.0	29.56
$PS_{14300}OH$	14.3	1.31	16.1	PS_{14300}-PLA_{3700}	18.0	1.19	3.7	20.55
$PS_{20000}OH$	20.0	1.07	23.9	PS_{20000}-PLA_{10000}	30.0	1.14	10.0	33.33
$PS_{40900}OH$	40.9	1.37	43.7	PS_{40900}-PLA_{4600}	45.5	1.29	4.6	10.11

[a,b]The M_n and M_w/M_n (molecular weight distribution) of PSOH or PS–PLA were characterized by GPC.
[c]The M_n of PSOH was obtained through end-group analysis from the ^{1}H-NMR spectrum: $M_{n[NMR]} = (3S_{\delta c = 1.46\ ppm}/2S_{\delta a} = 0.79\ ppm) \times 104 + 102$ and [OH]/[n-BuLi] = $3S_{\delta c} = 3.3\ ppm/2S_{\delta e} = 0.79\ ppm$.
[d]$M_n(PLA) = M_n(PS\text{–}PLA) - M_n(PSOH)$, as determined through GPC analysis.
[e]$f_{PLA} = M_n(PLA)/M_n(PS\text{–}PLA) \times 100\%$.
S_δ represents the integration of proton in different chemical environment of the polymer; $S_{\delta a}$ represents the integration the protons of CH3- in initiator part of PSOH; $S_{\delta c}$ represents the integration the protons in -CH(C6H5)-CH2- in PSOH; $S_{\delta e}$ represents the integration the protons in PS-CH2-CH2-OH.

DSC Q200 analysis (TA Corp.) from 0 to 140°C at 10°C/min. The surface morphology of the self-assembled PS–PLA films (spin-coated on silicon wafers with dimensions of 5 × 5 mm^2) was characterized by AFM (Nanoscope IIIa multimode scanning probe microscope) under an air atmosphere in tapping mode. The PS–PLA film peeled from the substrate was stuck on a sample stage and plated with platinum before SEM characterization, which was carried out on a Hitachi S-4700 scanning electron microscope at 20 kV and 10 mA.

RESULTS AND DISCUSSION

Characterization of PSOH and PS–PLA

The PS–PLA diblock copolymers were synthesized through a combination of living anionic polymerization and controlled ring-opening polymerization (Figure 1). The PSOH, prepared by *n*-BuLi-catalyzed living anionic polymerization and end-capped by EO, was coupled with a PLA block through the controlled ring-opening polymerization of D,L-lactide. $AlEt_3$ was used as a catalyst to convert PSOH into the aluminum alkoxide macroinitiator, which could be directly used to trigger the ring-opening polymerization. By regulating the amount of D,L-lactide used in the ring-opening polymerization or adopting PSOH with different molecular weights as a macroinitiator, we prepared five kinds of asymmetric PS–PLA samples with different f_{PLA}'s, as listed in Table I. The additional data in Table I indicate that when the molecular weight of PSOH was increased, f_{PLA} in PS–PLA decreased. This may have been due to the inverse relationship between the reaction activity of the —OH group and M_n of PSOH. PSOH with a lower molecular weight displayed a higher initiating activity.

To identify the PSOH and PS–PLA samples perspicuously, they were named $PS_{Mn}OH$ and PS_{Mn}–PLA_{Mn}, where the subscript *Mn* represents the number-average molecular weight of the chain, such as in $PS_{3900}OH$ and PS_{3900}–PLA_{3800}.

An IR spectral comparison between PSOH and PS–PLA is shown in Figure 2. For PSOH, chemical shift (H NMR) of various proton in polymer, $\sigma_{—OH} = 3500\ cm^{-1}$ reflected the terminated hydroxyl absorption, together with a series of four bands received at $\sigma_{C=C} = 1600$, 1585, 1500, and 1450 cm^{-1}(σ represents the IR absorption frequency of different functional groups in the polymer). These bands were the best evidence for the aromatic ring included in the PS block. Both the stretching vibrations of the aromatic ring skeleton and $\sigma_{C=O} = 1750$–1735 cm^{-1} of the ester carbonyl in PLA block were established in the IR spectra of PS–PLA; this suggested that both the PS and PLA block were involved in PS–PLA. These results indicate that D,L-lactide could be successfully initiated by the PSOH.

The linkage between the PS and PLA block could not be testified successfully with IR information only. Therefore, ^{1}H-NMR spectra of PS–PLA were obtained for further confirmation. The ^{1}H-NMR spectral comparison between PSOH and PS–PLA is presented in Figure 3. All of the ^{1}H-NMR resonances are reported in parts per million downfield from tetramethylsilane (0.0 ppm): PSOH: 1.58 ppm [m, —CH(C_6H_5)—CH_2—], 1.33 ppm (b, —CH_2— of initiator), 0.88 ppm (m, —CH_3 of initiator); $\delta(H_e) = 3.3$ ppm for the PS–CH_2—CH_2—OH {this was crucial to the calculation of [—OH]/[*n*-BuLi], and it was

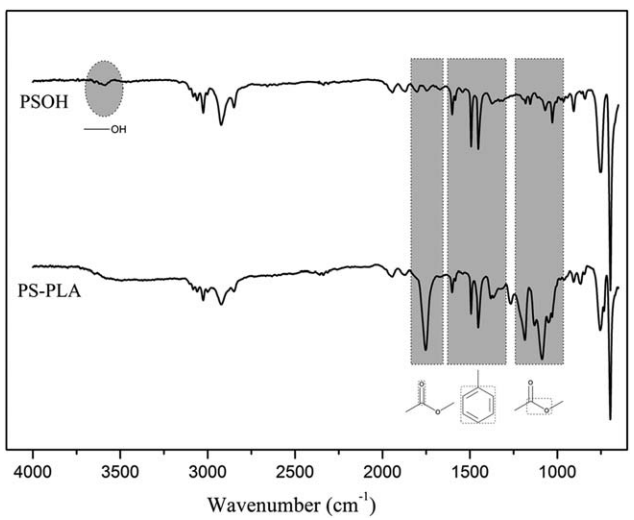

Figure 2. Comparison of the IR spectra between $PS_{3900}OH$ and PS_{3900}–PLA_{3800}.

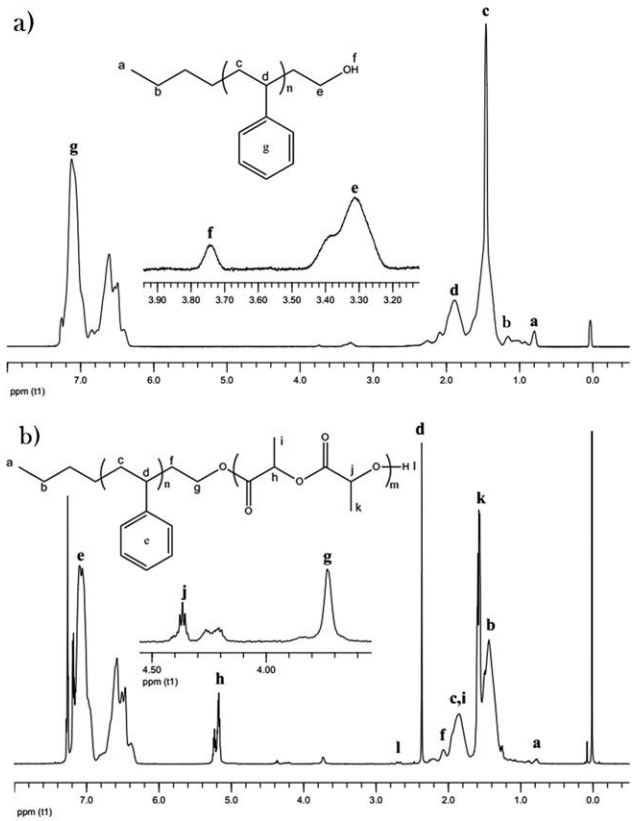

Figure 3. Comparison of the ^{1}H-NMR spectra between $PS_{3900}OH$ and PS_{3900}–PLA_{3800}: (a) $PS_{3900}OH$ and (b) PS_{3900}–PLA_{3800}. [Color figure can be viewed in the online issue, which is available at www.interscience.wiley.com.]

replaced by $\delta(H_g) = 3.8$ ppm of PS–CH_2—CH_2—O–PLA in the PS–PLA diblock copolymer}; PLA block in PS–PLA: $\delta(H_h) = 5.2$ ppm [m, —C(O)—C*H*(CH_3)—O—]; δ (H_i) = 1.6 ppm [—C(O)—CH(C*H*$_3$)—O—] (δ indicates the chemical shift (H NMR) of various proton in polymer).

For the synthesis of PSOH, different molar amounts of EO were used to investigate the effect of EO use on the terminal hydroxyl content of PSOH, which could be reflected by [—OH]/[*n*-BuLi]. As shown in Figure 4, [—OH]/[*n*-BuLi] increased gradually with increasing use of EO, but when the EO dose reached about 40 times [*n*-BuLi], [—OH]/[*n*-BuLi] reached a maximum of 0.84, which was slightly smaller than the theoretical value of 1. The excessive use of EO led to a decrease in the terminal hydroxyl content, which then gently tended to a constant at about 0.52. This may have been due to the oligomerization of the EO according to the investigation of Quirk.[35]

Self-Assembly of the PS–PLA Films

The chemical incompatibility between the PS and PLA blocks enabled the PS–PLA films to spontaneously self-assemble into microphase-separation structures with the lowest free energy. However, it was difficult to get long-range-ordered self-assembling nanostructures with reliance only on the inner superiority of mutual balance between the chemical incompatibility and covalent bond linkage of constituent blocks. External inducement, such as by thermal and solvent fields, were used to stimulate the self-assembling phase-separation process of the PS–PLA films.

Thermal-Field Regulation of the PS–PLA Films. Thermal annealing is thought to be a facile way to regulate the self-assembling of PS–PLA films. A thermal field provides energy for the thermodynamic movement of PS–PLA chains and thus promotes the reorganization of their conformation and orientation. The effect of the annealing temperature on the morphology of the PS–PLA film was investigated in this study, and it was reflected by SEM images of the PLA-component-etched PS–PLA film samples.

The self-assembling process of the amorphous PS–PLA involved the reorganization of both polymer segments and chains, although the segment adjustment was achieved only when the system temperature was higher than the T_g of PS–PLA. The thermodynamic properties of PS_{40900}–PLA_{4600} was determined by analysis with a DSC Q200 from TA Corp., in which the T_g of PS was thought to be 109.50°C and that of PLA was 69.65°C. Therefore, the thermal annealing of the PS–PLA film was carried out at 110 and 140°C, respectively.

Figure 5 shows the SEM images of the PS_{40900}–PLA_{4600} films thermally annealed at different temperatures after PLA was etched. Figure 5(a) shows the uniform nanopore morphology with a diameter (D) of 35 ± 3 nm dispersed on a smooth surface, but the pores were arranged randomly, and their quantity was scarce. However, Figure 5(b) shows a rough surface, uneven pore size distribution, and disordered pore arrangement. The disparate structures between Figure 5(a) and Figure 5(b) were attributed to the following reasons:

1. The etching of the PLA segment led to a nanoporous structure in the PS matrix film.
2. The low thermal annealing temperature and deficient annealing time led to randomly arranged and scarce nanopores [Figure 5(a)]. The thermal field thermostated at 110°C could not provide enough energy for the PS–PLA chains to overcome the energy barrier from located areas.[36] Moreover, the annealing period was too short for the

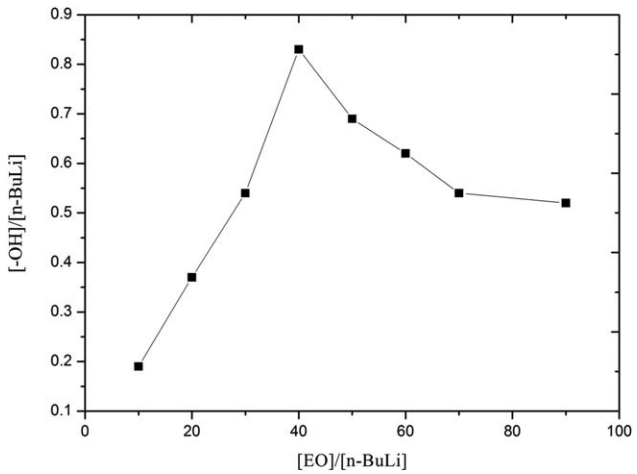

Figure 4. Relationship between the EO used in the PSOH synthesis and [—OH]/[*n*-BuLi].

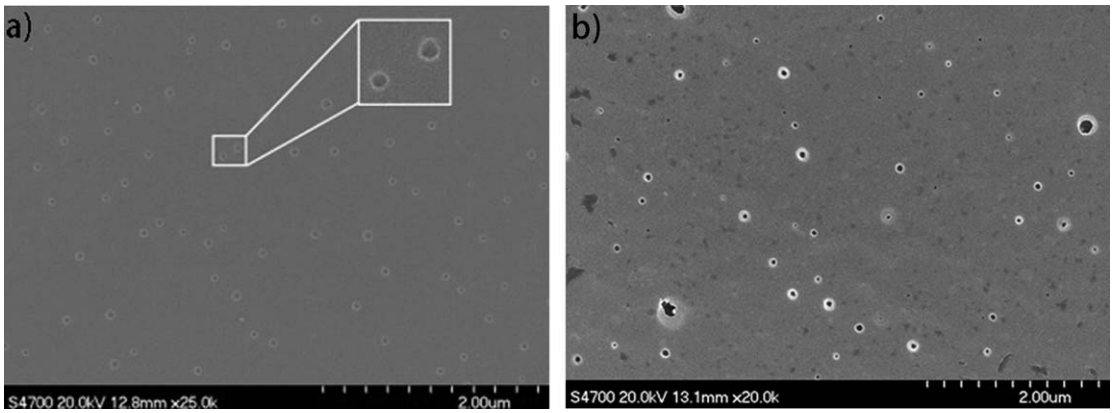

Figure 5. SEM images of the PLA-etched PS_{40900}–PLA_{4600} ($f_{PLA} = 10.11$) films thermally annealed at different temperatures for 4 h at (a) 110 and (b) 140°C.

polymer chains to reorganize their conformation and orientation completely. The PLA component buried in the depth of the self-assembled PS–PLA film resulted in sparse nanopores emerging among the film surface.

3. The rough surface and uneven pore size distribution in Figure 5(b) were attribute to the thermal degradation of the PLA segment because thermal annealing at 140°C was too hot for PS–PLA to self-assemble safely. We believe that the PLA chains degraded, and this resulted in the formation of PS homopolymer, which was incorporated into the PS matrix and caused an uncanny increase in the pore size.[18]

In summary, the temperature was critical for the thermal annealing of the PS–PLA films. A lower annealing temperature led to the impediment of segment conformation reorganization, whereas a higher temperature could result in PLA degradation and phase-separation structure defects. Thus, it was necessary to strike a balance between the annealing temperature and the annealing time for PS–PLA film thermal annealing.

Figure 6 manifests the surface morphologies of the PLA-component-etched PS–PLA films with different compositions after thermal annealing at 125°C for 9 h. We concluded that with the increase of f_{PLA} (8.09, 10.11, and 20.56%), the phase-

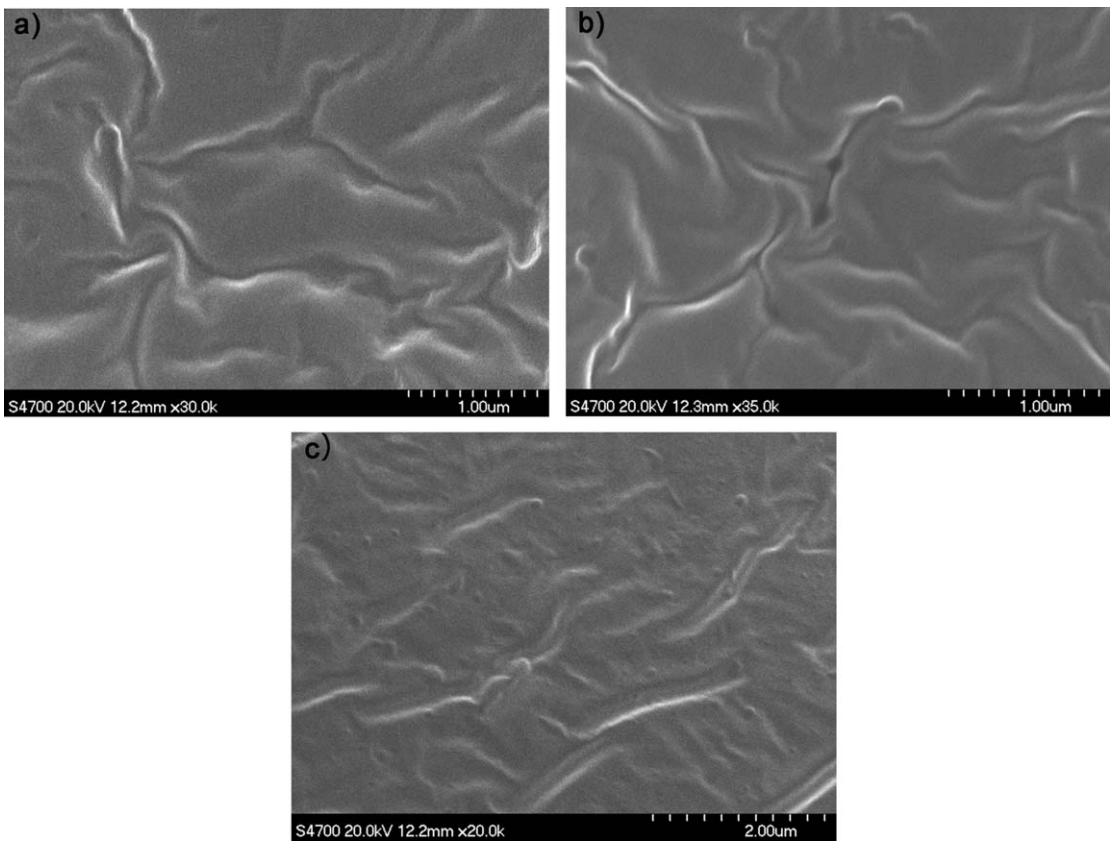

Figure 6. SEM images of the PLA-etched PS–PLA films with different compositions after thermal annealing at 125°C for 9 h: (a) PS_{40900}–PLA_{3600}, $f_{PLA} = 8.09\%$; (b) PS_{40900}–PLA_{4600}, $f_{PLA} = 10.11\%$; and (c) PS_{14300}–PLA_{3700}, $f_{PLA} = 20.56\%$.

Table II. Flory–Huggins Interaction Parameters between the PS/PLA Blocks and Different Solvents[5,7,27]

Solvent	$\chi_{PS-Solvent}$	$\chi_{PLA-Solvent}$	Solubility
Acetone	1.30	0.28	PLA-selective
Toluene	0.35	2.45	PS-selective
Chloroform	0.04	0.58	Neutral
Tetrahydrofuran	0.15	0.62	Neutral

separation structures of the PS–PLA altered from stripes disperse in a hole [Figure 6(a)] to a hole disperse in stripes [Figure 6(b)] to interleaved stripes [Figure 6(c)]. The first two types expressed a stripe–hole hybrid structure, in which the proportion of stripes and hole structures were the opposite, although the third type displayed an absolute stripe–interweave structure, which was uniformly distributed. It was thought that before PLA was etched, a smaller f_{PLA} would lead to a majority of PLA sphere phase-separation structures. With the increase of f_{PLA}, the PLA phase self-assembled into stripes parallel to the film surface, and such a structure was conducive to a reduction in the system energy.

The result in this part guaranteed that the phase-separation structures of the PS–PLA films could be regulated by the adjustment of the content of the PLA component in the PS–PLA diblock copolymer. Meanwhile, the PS–PLA film expressed many more diverse phase-separated structures after it was thermally annealed at 125°C for 9 h (stripes and holes) than after it was thermally annealed at 110°C for 4 h (holes). This also prevented the thermal degradation of the PLA component on the condition that the thermal annealing temperature was too high. However, only the long-range-ordered perpendicular oriented columns are applicable in the field of membrane separation, and the stripes–hole hybrid or stripes–interweave phase-separation structure obtained in this study are thought to have less use for this field.[37]

Solvent-Field Regulation of the PS–PLA Films. Solvent annealing is the most practical method for regulating the self-assembling of BCPs because it prevents the high melt viscosity involved in the thermal annealing process, in which polymer chains are incompetent to adjust their conformations. In a solvent field, the solvent molecules act as the plasticizers for polymer chain movement so that polymer chains can revise their conformation even below the T_g of PS–PLA.[38] Thus, the selection of the casting solvent and solvent evaporation were effective ways to dominate the regularity and orientation of phase-separate structures[39] during the spin-coating process.

Solvent selection. In view of the crucial impact of the solvent on the self-assembling of PS–PLA films right after spin-coating, two solvents were chosen as casting solvents on the basis of the interactions between the solvent molecules and the PS or PLA block. The miscibility between PS–PLA and the solvents could be reflected by polymer-solvent interaction parameters χ_{P-S} according to the Flory–Huggins model.[17,40] Then, solvent selectivity was assessed through the dates compared in Table II.

According to Flory–Huggins theory, a smaller χ_{P-S} ($\chi_{P-S} < 0.5$) indicates that the solvent has a better solubility for a certain polymer, whereas a larger one ($\chi_{P-S} > 0.5$) means that the polymer is relatively insoluble in the corresponding solvent. Thus, compared to PS, PLA was more soluble in acetone, and this was reflected by the larger $\chi_{PS-Acetone}$ and smaller $\chi_{PLA-Acetone}$. In this same way, toluene favored PS more than PLA. Although $\chi_{PS-Chloroform} > 0.5$, chloroform was still a good solvent for both the PS and PLA blocks, exhibiting only a small selectivity to PS.[41]

Solvent-evaporation-regulated PS–PLA self-assembly. Experiments attempting to perpendicularly orient the PLA phase-separation cylinders during film formation and self-assembly of the PS–PLA film were explored through the use of different solvents as casting solvents. The solvents from which the PS–PLA film was spin-coated could be divided into selective solvents (toluene) and neutral solvents (chloroform) because different χ_{P-S}'s led to different self-assembled transformation processes.

Solvent-evaporation model for PS–PLA self-assembly. Here, we first conceived a model for the film-forming and self-assembling process of PS–PLA in selective solvents before experimental validation (in toluene) and comparison (in chloroform). In this case, PS–PLA was dissolved in toluene (which favored PS) and then spin-coated onto silicon wafers. With the evaporation of toluene, the PS–PLA/toluene solution system experienced a process of Micelle deposition (PS–PLA) → Shell (PS) integration → Solvent path (PS) orientation → Core (PLA) integration → Perpendicular cylinder (PLA) formation.

Figure 7 shows a schematic diagram of this process, where, in the online figure, red represents the PS phase, green represents the PLA phase, blue represents the solvent, and brown represents the wafers. The PS–PLA molecules chains assembled into a micelle structure, in which the solvophobic PLA block shrank into a core and the solvophilic PS block swelled as the shell [Figure 7(a)]. With the evaporation of the solvent, the micelle concentration of this system increased and exceeded the micelle–gel concentration. The PS–PLA micelles stacked into a hexagonally packed micelle–film morphology according to the minimum energy principle. The cross-sectional view of the micelle–film illustrated that the adjacent micelle–shells were likely to merge gradually because they were chemically unanimous. Countless solvent-evaporation channels came into being after the micelle–shells merged [Figure 7(b)]. The distribution of selective solvent in the PS–PLA micelles was indicated by the coordinates established in the micellar cross section: where the abscissa represents the reference distance (d), the maximum of which is equal to the micelle radius (R), and the ordinate represents the concentration of solvent. The increase in d resulted in a dramatic rise in the solvent concentration because PLA was solvophobic in toluene and PS was relatively solvophilic [Figure 7(c)]. During the film-forming process, solvent molecules escaped from the micelle–shell channels in the direction perpendicular to the film surface. This procedure promoted further merging of the PS shells and PLA cores also showed a tendency toward mutual integration [Figure 7(d)]. The PLA cores integrated with each other, and stringlike PLA bands formed gradually with the evaporation of the solvent. Both the PS and PLA blocks reorganized their orientation perpendicular to the film

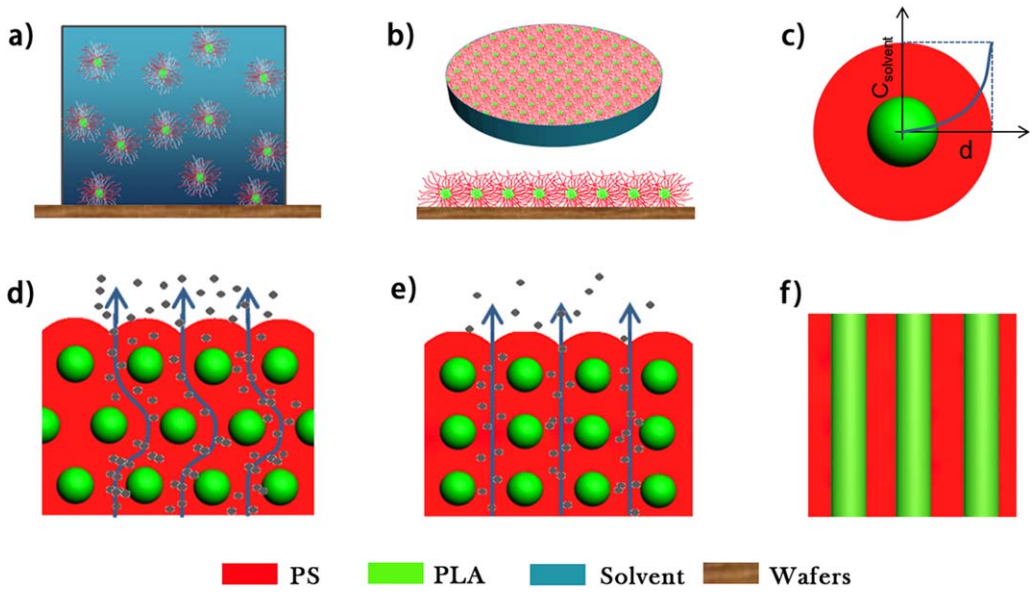

Figure 7. Schematic diagram of the micelle–integration inducement on the vertical-column phase-separation structure formation during PS–PLA film formation in selective solvents. [Color figure can be viewed in the online issue, which is available at wileyonlinelibrary.com.]

surface [Figure 7(e)]. The PS–PLA film self-assembled into long-range-ordered phase-separation structures, in which the segregated PLA columns were dispersed in a continuous matrix of PS domains [Figure 7(f)].

As indicated in this model, the film-forming process and self-assembling process of PS–PLA in toluene solvent were mainly facilitated by the interactions between polymer blocks and solvent molecules. Specifically, solvent evaporation kinetically trapped polymer blocks oriented perpendicular to the surface. We contemplated that the vertical driving force derived from solvent evaporation would also take effect when the PS–PLA experienced the film-forming and self-assembling processes in neutral solvents such as chloroform. Although the promoting effect of the micelle structure on the self-assembling process was absent, a vertical-column phase-separation structure was also formed in the PS–PLA/neutral solvent system.

Solvent self-assembly of the PS–PLA film. Toluene and chloroform were chosen as the casting solvents for the spin-coating of the asymmetric PS–PLA samples (PS_{14300}–PLA_{6000} and PS_{14300}–PLA_{3700}). Then, the as-spun films were placed in open air at 25°C for solvent evaporation. The relationship between solvent selection and the phase-separation structures was investigated.

The composition of the PS–PLA diblock copolymer had an important influence on the size and density of the PS–PLA film phase-separation structures. The comparison between the AFM images in Figures 8(a,c) and 8(b,d) indicate that a higher f_{PLA} (29.56%) in PS_{14300}–PLA_{6000} led to rich and high-density surface morphologies, whereas a lower f_{PLA} (20.56%) in the PS_{14300}–PLA_{3700} film expressed simple and clear but few surface morphologies in holes and protrusion phase-separation structures. The images in Figures 8(a,b) and 8(c,d) display the surface morphology of the PS–PLA self-assembled in toluene and chloroform, respectively. Toluene had a better selectivity for the PS phase than chloroform; thus, the PS blocks in Figure 8(a,b) were better trapped by the driving force derived from toluene evaporation, which exhibited many visible and clear protrusion structures, indicated that the solvent could trap the vertical-column phase-separation structures.[27] However, in neutral solvents such as chloroform, the PS–PLA polymer chains were totally disordered because chloroform mediated unfavorable enthalpy interactions between the PS and PLA blocks.[5] During the chloroform evaporation process, both of the two blocks in PS–PLA were trapped by the absconding of solvent molecules and shifting to the surface of the film; this led to continuous up-and-down protrusions alternating with a few pore structures, as shown in Figure 8(c,d). Thus, the solvent showed big differences between the solvent–polymer parameters among each block of the BCPs ($\chi_{PS-Toluene} = 0.35$, $\chi_{PLA-Toluene} = 2.45$, $\chi_{PS-Chloroform} = 0.04$, $\chi_{PLA-Chloroform} = 0.58$), which tended to form significant phase-separation structures. Furthermore, with the evaporation of such a solvent, the polymer blocks were selectively trapped in the perpendicular directions to form the classic vertical-column phase-separation structures.

However, because of the faster evaporation of the solvent or the magnanimous solvent evaporation during the spin-coating process, only a little solvent was left to mediate the unfavorable interactions between the polymer blocks or trap the migrating blocks gently. That may have been why the phase-separation structures formed in Figure 8 were sparse and disordered. This conclusion shows that solvent evaporation promoted the formation of vertical-column phase-separation structure during the film-forming and self-assembling process of PS–PLA, but the ordering and perfection of this structure mainly depended on the self-assembling features derived from the incompatibility between the different blocks.

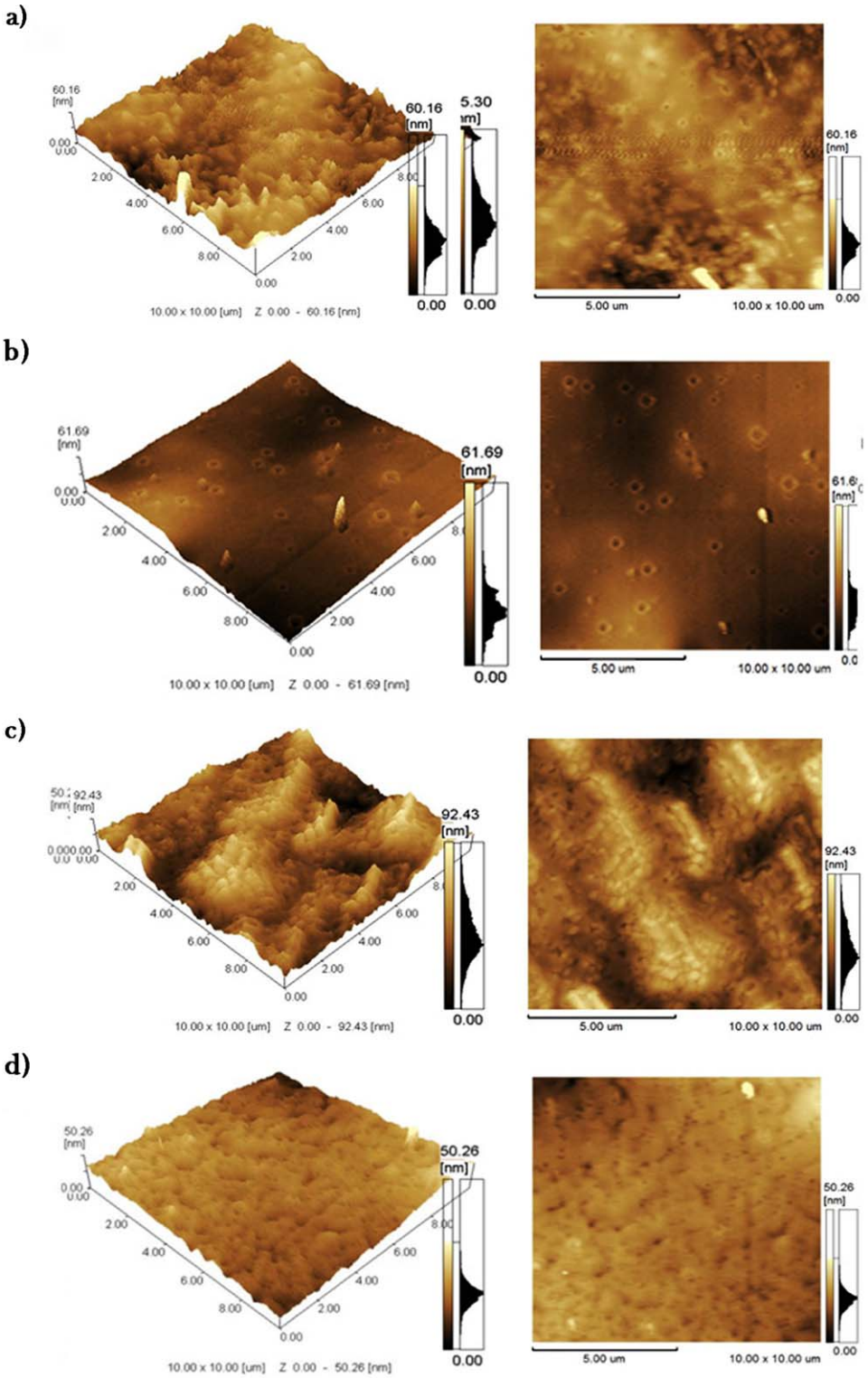

Figure 8. AFM images of the PS–PLA thin films spin-coated with different solvents and dried in open air at 25°C: (a) PS_{14300}–PLA_{6000}/toluene, $f_{PLA} = 29.56\%$; (b) PS_{14300}–PLA_{3700}/toluene, $f_{PLA} = 20.56\%$; (c) PS_{14300}–PLA_{6000}/chloroform, $f_{PLA} = 29.56\%$; and (d) PS_{14300}–PLA_{3700}/chloroform, $f_{PLA} = 20.56\%$. [Color figure can be viewed in the online issue, which is available at wileyonlinelibrary.com.]

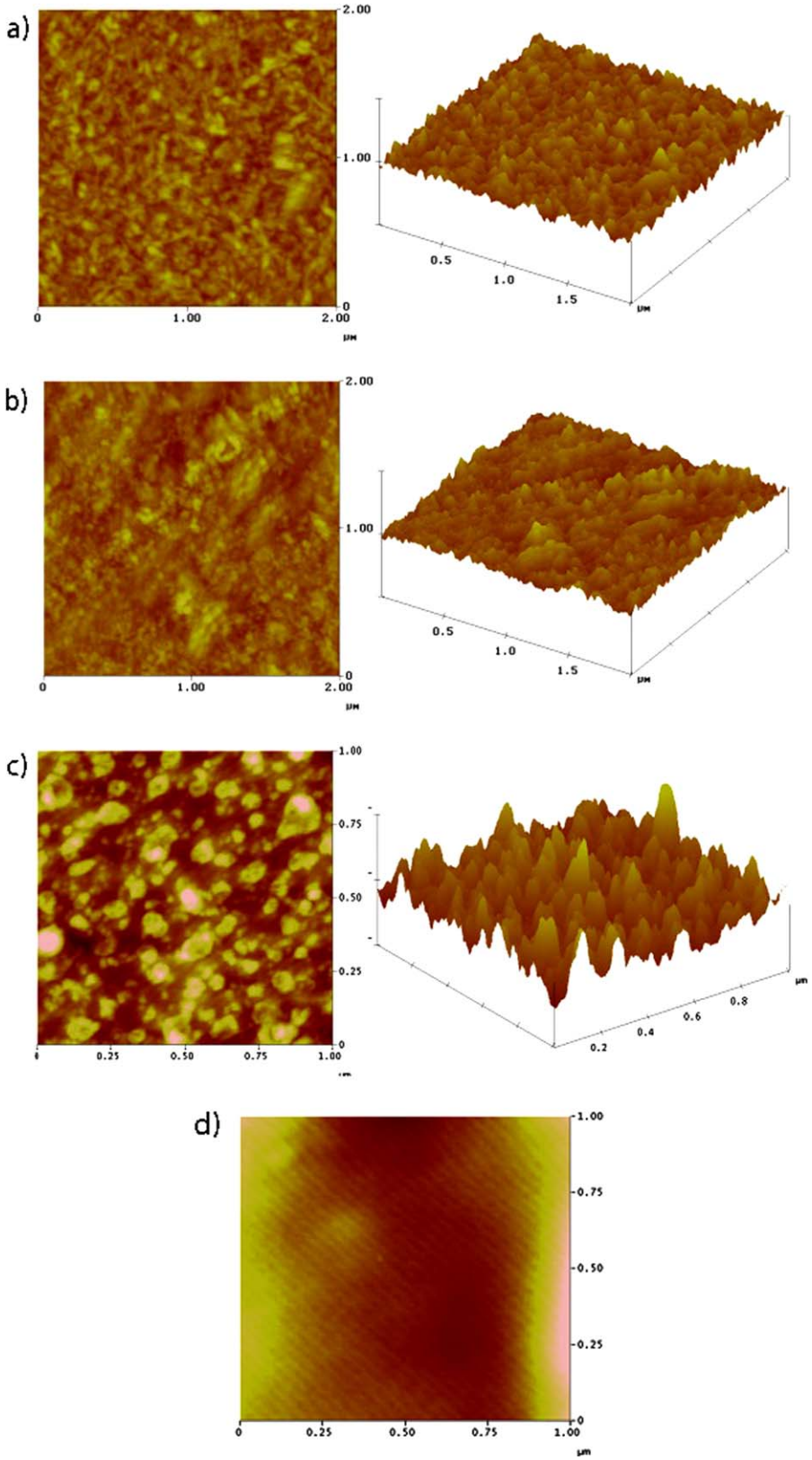

Figure 9. AFM images of the PS_{20000}–PLA_{10000} film solvent-annealed at 40°C in toluene for different periods: (a) 5, (b) 7, (c) 12, and (d) 24 h. [Color figure can be viewed in the online issue, which is available at wileyonlinelibrary.com.]

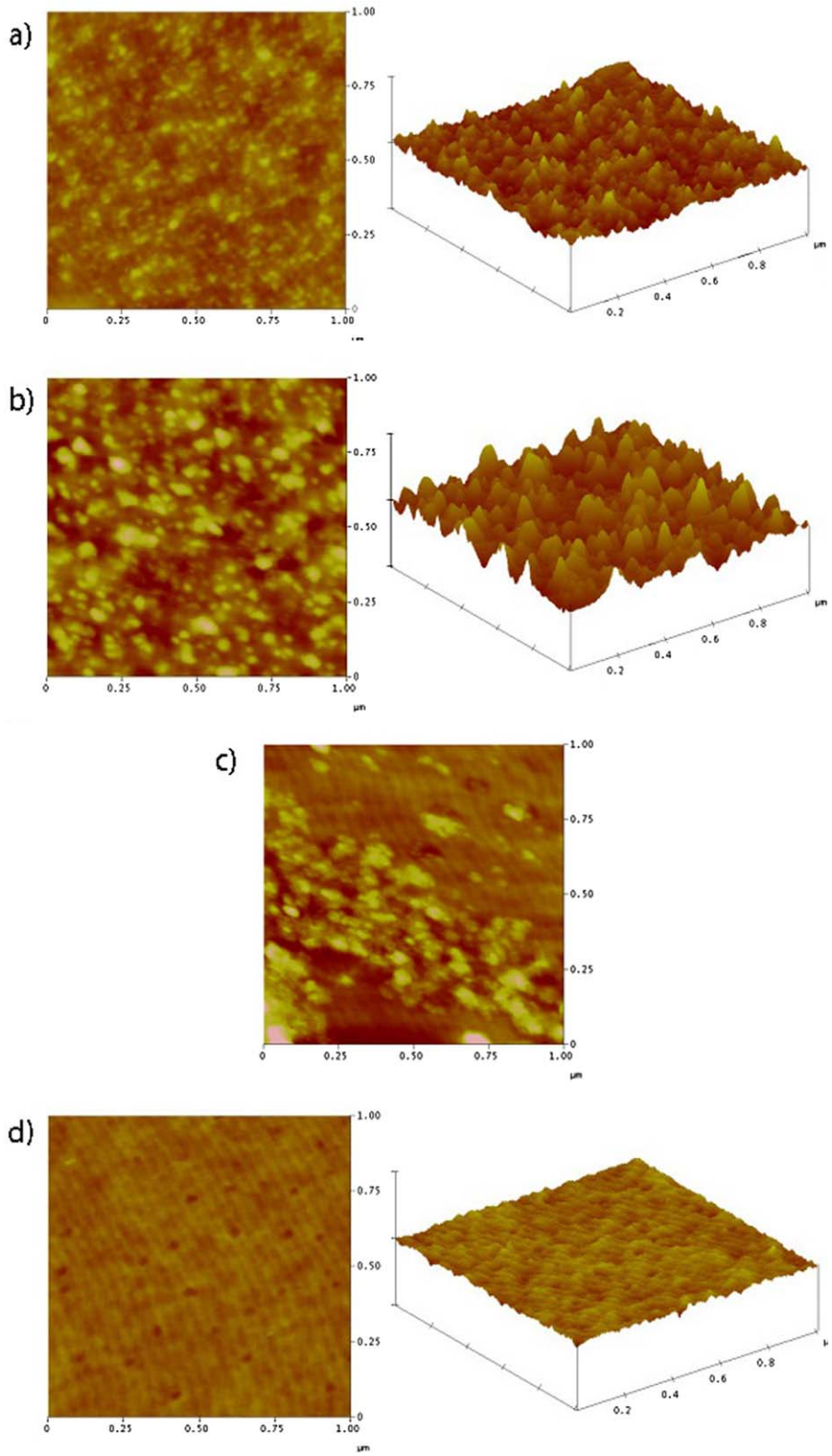

Figure 10. AFM images of the PS_{20000}–PLA_{10000} film solvent-annealed at 40°C in THF for different periods: (a) 5, (b) 7, (c) 12, and (d) 24 h. [Color figure can be viewed in the online issue, which is available at wileyonlinelibrary.com.]

Solvent annealing. Solvent annealing was always implemented by the suffocation of the PS–PLA films under a saturated solvent-vapor environment. This was a process that enhanced the mobility of the polymer chains by both plasticization of the polymer blocks and attenuation of the unfavorable enthalpy interactions between the different blocks. Because the ordering and modification of the

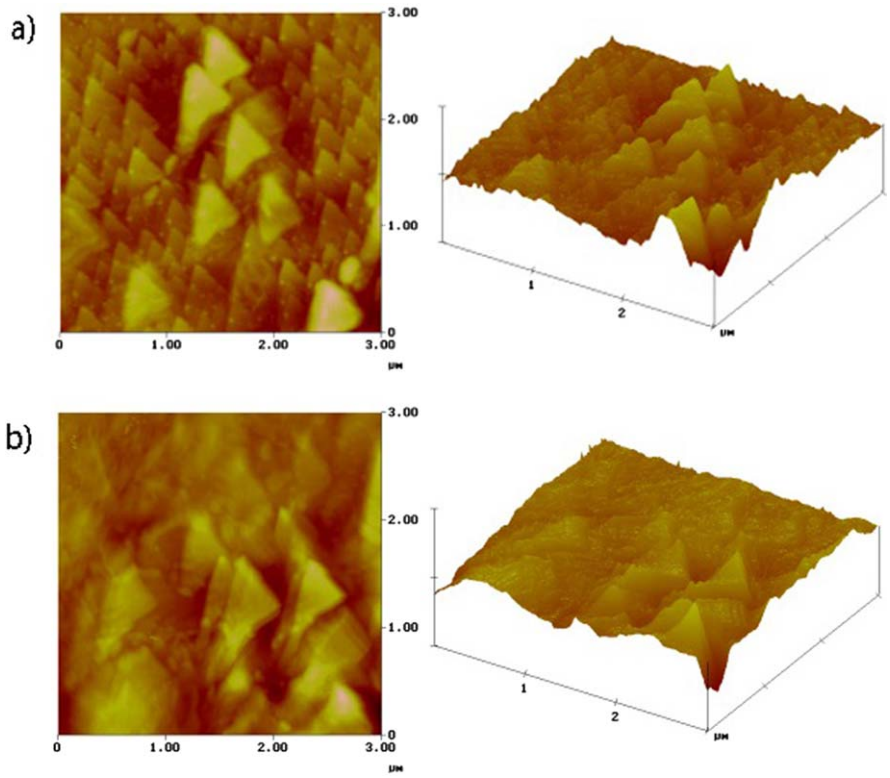

Figure 11. AFM images of the PS_{20000}–PLA_{10000} film annealed at 40°C in acetone for different periods: (a) 7 and (b) 17 h. [Color figure can be viewed in the online issue, which is available at wileyonlinelibrary.com.]

PS–PLA film phase-separation structures require the extension of the self-assembling period and adequate power for segment reorganization, solvent annealing in this study was performed by the retention of the PS–PLA films in closed beakers possessed with a constant solvent vapor at 40°C for different periods.

Figure 9 shows the AFM images of the PS–PLA film solvent-annealed in toluene vapor at 40°C for different periods. A nucleation–growth mechanism could be used to explain the phase-separation process of the PS–PLA film shown in Figure 9. The PS–PLA films exhibited different surface morphologies with the extension of the solvent-annealing time; these evolved into single oriented stripes parallel to the film surface. Uniform PS tapers were formed on the surface of the PS–PLA film under a toluene-vapor atmosphere [Figure 9(a)]. This indicated that the PS blocks exhibited a better mobility than PLA at the interface between the film and toluene vapor; this enabled them migrate from the film–matrix to the film surface to form PS tapers. With the extension of annealing time, more and more PS blocks migrated to the film surface, and the PS tapers became taller and thicker [Figure 9(b,c)]. The solvent-annealing time was extended to 24 h [Figure 9(d)]. The taper structures of PS (67% of PS–PLA) connected into single oriented strips to reduce the surface energy. This process indicated that when one of the blocks exhibited a preferential affinity to the solvent vapor, prolonged solvent annealing would lead to parallel-stripe phase-separation structures in the PS–PLA film.[42] The phase-separation nucleus under this circumstance primarily formed at the vapor/film interface and subsequently diffused into the film bulk.

Figure 10 shows the AFM images of the PS–PLA film solvent-annealed in THF vapor at 40°C for different periods. When the solvent-annealing process was performed under THF vapor, the PS–PLA film exhibited a similar evolution process to the toluene-vapor annealing process. A uniform taper structure was formed after the PS–PLA was annealed in THF vapor for 5 h [Figure 10(a)]. The density of the taper structure was scarce compared to the counterpart surface morphology in toluene vapor. The taper structure became taller and thicker when the annealing time was extended to 7 h, and this phenomenon was constant in the toluene-vapor-treated PS–PLA films [Figure 10(b)]. Fortunately, the transition form of the taper and strip was observed after the annealing time was extended to 12 h, in which time the taper and strip structures coexisted in the PS–PLA film [Figure 10(c)]. The taper structure subsided when the annealing time was extended to 24 h. Long-range-ordered and single oriented stripes were exposed at the surface of the PS–PLA film [Figure 10(d)]. Generally, THF brought a much higher saturated vapor pressure than toluene at 40°C; this resulted in many exquisite and clear phase-separation structures compared to those observed in the toluene-vapor annealing process. Moreover, a comparison between Figures 9(c) and 10(c) shows that the taper–strip transition process developed much faster when the PS–PLA film was annealed in THF vapor rather than in toluene. This was because the PS–PLA film surface was completely swelled by THF vapor, and the increase in free volume effectively reduced the energy barrier of polymer reorganization and increased the motion capability of the PS and PLA chains.

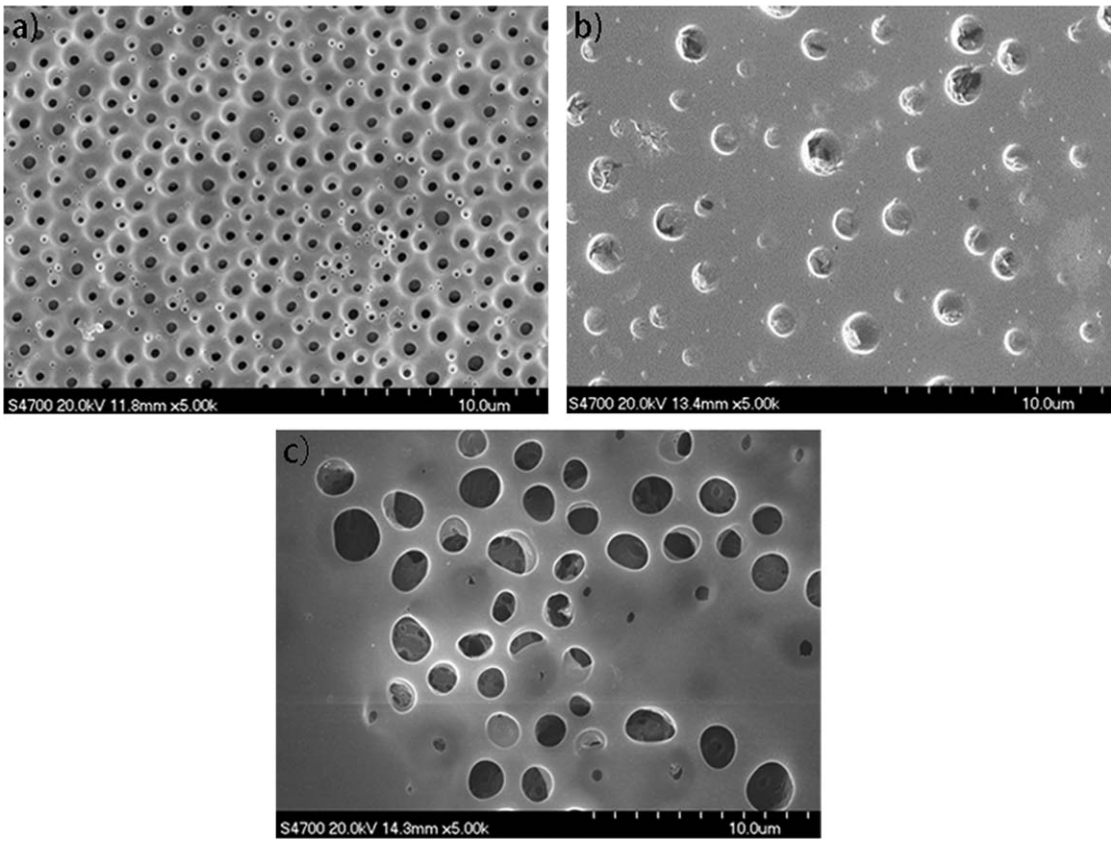

Figure 12. SEM images of toluene-solvent-evaporation-regulated PS–PLA films with different f_{PLA}'s after PLA was chemically etched for 15 days at 40°C: f_{PLA} = (a) 10.11, (b) 33.33, and (c) 49.35%.

Figure 11 shows the AFM images of the PS–PLA film solvent-annealed in acetone vapor at 40°C for 7 and 17 h, respectively. During the solvent-annealing process, the PS–PLA film was swollen by the saturated acetone-vapor molecules, which displayed a strong selection effect on the PLA segment. In this role, the ordered PLA phase nucleated at the interface between the polymer film surface and the vapor phase, and this gradually formed a taper structure [Figure 11(a)]. With the time extension of acetone annealing, the ordered phase-separation structures grew at the metastable disordered phase and extended to the periphery [Figure 11(b)]. A featureless film surface of PLA was generated because the surface energy was thought to be lower than PS.[18]

Etching of PLA in the PS–PLA Films. Because the PS phase was insoluble in alkaline solution where PLA could be effectively hydrolyzed, the chemical etching of the PLA component from the PS matrix could be applied to prepare nanoporous membranes. To corroborate that the pore size of the PLA-etched PS–PLA films could be regulated by the content of the PLA component in the PS–PLA diblock copolymer, PS–PLA films with different PLA components were self-assembled under solvent-evaporation inducement followed by the chemical etching of the PLA segment in alkaline solution.

Figure 12 shows the SEM images of the PLA-etched PS–PLA films self-assembled by solvent (toluene) evaporation. We concluded that with the increase in the PLA component in the PS–PLA raw polymer, the pore size of the PLA-etched PS–PLA films was amplified gradually. However, the pore distribution of these films was relatively disordered. The average D values of the pore structures in Figure 12(a–c) were estimated to be 500, 1500, and 1900 nm, respectively. This may have been due to the inadequate block reorganization during the solvent-evaporation inducement. During the solvent-annealing process, because of the selective features of toluene, which lead to single-phase ordered nucleation at the interface between the film surface and the solvent vapor, the toluene-vapor annealing of the PS–PLA films brought many more ordered phase-separation structures. Such a conjecture was affirmed by the SEM image of the PLA-etched PS–PLA self-assembled in the toluene-vapor circumstance, as shows in Figure 13.

A long-range-ordered hexagonally packed nanoporous PS membrane was finally achieved after the PLA segment chemically etched from the solvent (toluene)-annealed PS–PLA film was perpendicularly oriented to the PLA column phase-separation structure dispersed in the continuous PS matrix. The nanoporous PS membrane exhibited a diameter (D) of about 500 nm and a center-to-center distance (d^*_{c-c}) of about 1700 nm.

However, some problems occurred during the etching process:***

1. The PS–PLA films separated easily from substrate in alkaline solution; these were cautiously picked up from the alkaline

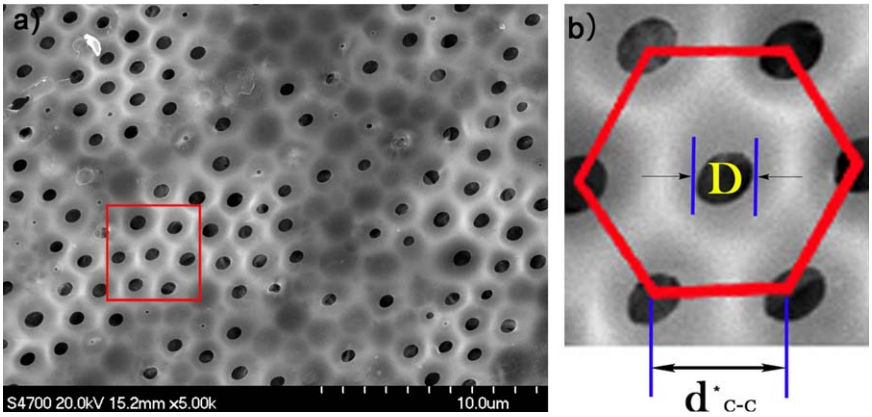

Figure 13. SEM images of the toluene-vapor-annealed PS–PLA ($f_{PLA} = 10.11\%$) films after the PLA segment was etched: (a) overall view of the long-range-ordered, hexagonally packed nanoporous PS membrane and (b) porous structure diagram. [Color figure can be viewed in the online issue, which is available at wileyonlinelibrary.com.]

solution with a slide support, rinsed thoroughly, and dried for SEM analysis. The abscission of the PS–PLA films from the substrate were attributed to the fact that the substrate exhibited more affinity to the PLA phase than to PS. This means that PLA was prior to wet the substrate during spin-coating and self-assembling process. A PLA wealthy polymer/substrate interface is usually formed in this way. Serious degradation occurring in such an interface led to the abscission of the PS–PLA film from the substrate during the PLA etching process.[17] Fortunately, substrate surface grafting treatment is thought to be a promising solution to this problem.

2. The PS–PLA films were very prone to generating cracks or even resulting in fracture in the entire film. The fragmentation was not only attributed to the residual stress or brittleness of the PS–PLA itself but also to the deformed pores being connected to one to another during the degradation process, as evidenced by the SEM images with larger distributions of pore size.

CONCLUSIONS

Asymmetric PS–PLA diblock copolymers with different f_{PLA}'s were prepared as precursors for the self-assembly of PS–PLA films. PSOH with a lower molecular weight displayed a higher initiating activity because of the reactivity of the —OH group in PS–PLA.

The phase-separated morphologies of the PS–PLA films could be regulated by solvent evaporation or thermal or solvent annealing. Thermal annealing of the PS–PLA film performed at a proper temperature (125°C) indicated that the phase-separation morphologies of the PS–PLA films could be regulated through the adjustment of the content of the PLA component, in which a smaller f_{PLA} led to a majority of PLA sphere phase-separation structures, whereas an increase in f_{PLA} resulted in PLA stripes interwoven in the film surface. A lower annealing temperature resulted in a sparse pore structure, and a higher temperature led to an uneven pore size distribution or even defects on the film surface. Thus, the thermal annealing of the PS–PLA films was always restricted by PLA degradation and the high melt viscosity, in which the polymer chains were incompetent to adjust their conformations.

Under the solvent-evaporation system, either a neutral or selective solvent could kinetically trap the polymer blocks oriented perpendicular to the film surface; this generated a vertical-cylinder phase-separation structure. The PS (shell)–PLA (core) micelle structure involved in the selective solvent-evaporation system was thought to be another feature that promoted the formation of the vertical-cylinder structure. Selective solvent (toluene) evaporation generated visible and clear protrusion structures because toluene had a preferential affinity to PS, whereas neutral solvent (chloroform) evaporation brought about continuous up-and-down structures because both of the two blocks in PS–PLA were trapped in the film surface. Generally, solvent evaporation did promote the formation of the vertical-column phase-separation structure during the film-formation and self-assembly processes, but the ordering and perfecting of this structure mainly depended on the self-assembly features derived from the incompatibility between the different blocks.

During the solvent-annealing process, the PS–PLA film surface was completely swollen by solvent vapor, and an increase in the free volume effectively reduced the energy barrier of polymer reorganization and increased the motion capability of the PS and PLA chains. A vertical-column phase-separation structure was generated whether the PS–PLA film was annealed in toluene or THF vapor. THF generated a much more exquisite and clear taper structure than toluene because it brought a higher saturated vapor pressure than toluene at 40°C, but toluene brought a much more ordered phase-separation structure because of its selective feature to PS phase, which resulted in a single phase-ordered nucleation at the interface between the film surface and the solvent vapor. The taper–strip transition process was detected both in the toluene- and THF-vapor annealing processes, and this morphology transition developed much faster in THF because it brought a higher saturated vapor pressure than toluene at 40°C.

PS membranes with ordered periodic nanoporous structures were obtained by the selective etching of segregated PLA domains dispersed in a continuous matrix of PS. A nanoporous membrane with a narrow pore size distribution was obtained from the cylindrical morphology formed in the PS–PLA films after the chemical etching of the PLA segment, with PS left as the matrix.

ACKNOWLEDGMENTS

This project was supported by Fundamental Research Funds for the Central Universities (contract grant number ZZ1209).

REFERENCES

1. Matsen, M.; Bates, F. *Macromolecules* **1996**, *29*, 1091.
2. Lynd, N. A.; Meuler, A. J.; Hillmyer, M. A. *Prog. Polym. Sci.* **2008**, *33*, 875.
3. Krausch, G.; Magerle, R. *Adv. Mater.* **2002**, *14*, 1579.
4. Li, H.-W.; Huck, W. T. *Nano Lett.* **2004**, *4*, 1633.
5. Rzayev, J.; Hillmyer, M. A. *J. Am. Chem. Soc.* **2005**, *127*, 13373.
6. Sidorenko, A.; Tokarev, I.; Minko, S.; Stamm, M. *J. Am. Chem. Soc.* **2003**, *125*, 12211.
7. Phillip, W. A.; O'Neill, B.; Rodwogin, M.; Hillmyer, M. A.; Cussler, E. *ACS Appl. Mater. Interfaces* **2010**, *2*, 847.
8. Li, X.; Fustin, C.-A.; Lefèvre, N.; Gohy, J.-F.; De Feyter, S.; De Baerdemaeker, J.; Egger, W.; Vankelecom, I. F. *J. Mater. Chem.* **2010**, *20*, 4333.
9. Yang, S. Y.; Yang, J.-A.; Kim, E.-S.; Jeon, G.; Oh, E. J.; Choi, K. Y.; Hahn, S. K.; Kim, J. K. *ACS Nano* **2010**, *4*, 3817.
10. Nuxoll, E. E.; Hillmyer, M. A.; Wang, R.; Leighton, C.; Siegel, R. A. *ACS Appl. Mater. Interfaces* **2009**, *1*, 888.
11. Koneripalli, N.; Singh, N.; Levicky, R.; Bates, F. S.; Gallagher, P. D.; Satija, S. K. *Macromolecules* **1995**, *28*, 2897.
12. Albert, J. N. L.; Epps, T. H., *III. Mater. Today* **2010**, *13*, 24.
13. Segalman, R. A. *Mater. Sci. Eng. R* **2005**, *48*, 191.
14. Luo, M.; Seppala, J. E.; Albert, J. N. L.; Lewis, R. L.; Mahadevapuram, N.; Stein, G. E.; Epps, T. H. *Macromolecules* **2013**, *46*, 1803.
15. Morkved, T.; Lu, M.; Urbas, A.; Ehrichs, E.; Jaeger, H.; Mansky, P.; Russell, T. *Science* **1996**, *273*, 931.
16. Zalusky, A. S.; Olayo-Valles, R.; Wolf, J. H.; Hillmyer, M. A. *J. Am. Chem. Soc.* **2002**, *124*, 12761.
17. Vayer, M.; Hillmyer, M. A.; Dirany, M.; Thevenin, G.; Erre, R.; Sinturel, C. *Thin Solid Films* **2010**, *518*, 3710.
18. Olayo-Valles, R.; Guo, S.; Lund, M.; Leighton, C.; Hillmyer, M. A. *Macromolecules* **2005**, *38*, 10101.
19. Mark, J. E. *Acc. Chem. Res.* **2006**, *39*, 881.
20. David I. Bower. Cambridge University Press: Cambridge, 0521631378 - An Introduction to Polymer Physics, Cambridge, 2002. Chapter 3, **2002**, 63.
21. Fukunaga, K.; Elbs, H.; Magerle, R.; Krausch, G. *Macromolecules* **2000**, *33*, 947.
22. Mansky, P.; Liu, Y.; Huang, E.; Russell, T.; Hawker, C. *Science* **1997**, *275*, 1458.
23. Kim, S. H.; Misner, M. J.; Xu, T.; Kimura, M.; Russell, T. P. *Adv. Mater.* **2004**, *16*, 226.
24. Garcia, I.; Tercjak, A.; Gutierrez, J.; Rueda, L.; Mondragon, I. *J. Phys. Chem. C* **2008**, *112*, 14343.
25. Huang, H.; Hu, Z.; Chen, Y.; Zhang, F.; Gong, Y.; He, T.; Wu, C. *Macromolecules* **2004**, *37*, 6523.
26. Tokarev, I.; Krenek, R.; Burkov, Y.; Schmeisser, D.; Sidorenko, A.; Minko, S.; Stamm, M. *Macromolecules* **2005**, *38*, 507.
27. Phillip, W. A.; Hillmyer, M. A.; Cussler, E. L. *Macromolecules* **2010**, *43*, 7763.
28. Yang, S. Y.; Ryu, I.; Kim, H. Y.; Kim, J. K.; Jang, S. K.; Russell, T. P. *Adv. Mater.* **2006**, *18*, 709.
29. Elbs, H.; Drummer, C.; Abetz, V.; Krausch, G. *Macromolecules* **2002**, *35*, 5570.
30. Burgess, F.; Cunliffe, A.; Richards, D.; Sherrington, D. *J. Polym. Sci. Polym. Lett. Ed.* **1976**, *14*, 471.
31. Kricheldorf, H. R.; Kreiser-Saunders, I.; Jürgens, C.; Wolter, D. *Macromol. Symp.* **1996**, *103*, 85.
32. Nam, J. Y.; Sinha Ray, S.; Okamoto, M. *Macromolecules* **2003**, *36*, 7126.
33. Sinha Ray, S.; Maiti, P.; Okamoto, M.; Yamada, K.; Ueda, K. *Macromolecules* **2002**, *35*, 3104.
34. Hadjichristidis, N.; Pispas, S.; Floudas, G. Block Copolymers, Synthetic Strategies, Physical Properties and Applications; Wiley: New York, **2003**.
35. Quirk, R. P.; Mathers, R. T.; Wesdemiotis, C.; Arnould, M. A. *Macromolecules* **2002**, *35*, 2912.
36. Mark, J. E. *Acc. Chem. Res.* **2004**, *37*, 946.
37. Ruiz, R.; Kang, H.; Detcheverry, F. A.; Dobisz, E.; Kercher, D. S.; Albrecht, T. R.; de Pablo, J. J.; Nealey, P. F. *Science* **2008**, *321*, 936.
38. Peng, J.; Kim, D. H.; Knoll, W.; Xuan, Y.; Li, B.; Han, Y. *J. Chem. Phys.* **2006**, *125*, 064702.
39. Ho, R.-M.; Tseng, W.-H.; Fan, H.-W.; Chiang, Y.-W.; Lin, C.-C.; Ko, B.-T.; Huang, B.-H. *Polymer* **2005**, *46*, 9362.
40. Chen, Y.; Huang, H.; Hu, Z.; He, T. *Langmuir* **2004**, *20*, 3805.
41. Böker, A.; Müller, A. H.; Krausch, G. *Macromolecules* **2001**, *34*, 7477.
42. Van Dijk, M.; Van den Berg, R. *Macromolecules* **1995**, *28*, 6773.